ISSN 1674-1056
http://cpb.iphy.ac.cn
http://iopscience.iop.org/cpb
中国物理 B
Chinese Physics
中国物理 Chinese Physics B

Lamb wave signal selective enhancement by an improved design of meander-coil electromagnetic acoustic transducer

Wen-Xiu Sun(孙文秀), Guo-Qiang Liu(刘国强), Hui Xia(夏慧), Zheng-Wu Xia(夏正武)

Citation: Chin. Phys. B . 2018, 27(8): 084301. **doi:** 10.1088/1674-1056/27/8/084301

Journal homepage: http://cpb.iphy.ac.cn; http://iopscience.iop.org/cpb

What follows is a list of articles you may be interested in

Generation of narrowband Lamb waves based on the Michelson interference technique

Tian-Ming Ye(叶天明), Yan-Feng Xu(徐琰锋), Wen-Xiang Hu(胡文祥)

Chin. Phys. B . 2018, 27(5): 054301. **doi:** 10.1088/1674-1056/27/5/054301

Wideband dispersion removal and mode separation of Lamb waves based on two-component laser interferometer measurement

Yan-Feng Xu(徐琰锋), Wen-Xiang Hu(胡文祥)

Chin. Phys. B . 2017, 26(9): 094301. **doi:** 10.1088/1674-1056/26/9/094301

Selective generation of ultrasonic Lamb waves by electromagnetic acoustic transducers

Ming-Liang Li(李明亮), Ming-Xi Deng(邓明晰), Guang-Jian Gao(高广健)

Chin. Phys. B . 2016, 25(12): 124301. **doi:** 10.1088/1674-1056/25/12/124301

Quantitative damage imaging using Lamb wave diffraction tomography

Hai-Yan Zhang(张海燕), Min Ruan(阮敏), Wen-Fa Zhu(朱文发), Xiao-Dong Chai(柴晓冬)

Chin. Phys. B . 2016, 25(12): 124304. **doi:** 10.1088/1674-1056/25/12/124304

Interface-guided mode of Lamb waves in a two-dimensional phononic crystal plate

Huang Ping-Ping, Yao Yuan-Wei, Wu Fu-Gen, Zhang Xin, Li Jing, Hu Ai-Zhen

Chin. Phys. B . 2015, 24(5): 054301. **doi:** 10.1088/1674-1056/24/5/054301

Lamb wave signal selective enhancement by an improved design of meander-coil electromagnetic acoustic transducer*

Wen-Xiu Sun(孙文秀)[1,2], Guo-Qiang Liu(刘国强)[1,2,†], Hui Xia(夏慧)[1], and Zheng-Wu Xia(夏正武)[1]

[1] *Institute of Electrical Engineering, Chinese Academy of Sciences, Beijing* 100190, *China*
[2] *School of Electronic, Electrical and Communication Engineering, University of Chinese Academy of Sciences, Beijing* 101408, *China*

(Received 25 March 2018; revised manuscript received 26 April 2018; published online 10 July 2018)

In this paper, we investigate a method of selectively enhancing the single mode signal of a Lamb wave by using a meander-coil electromagnetic acoustic transducer (EMAT) with a new magnetic configuration. We use the Lamb antisymmetric (A0) mode and symmetric (S0) mode as an example for analysis. The analytical expression of the magnitude of the spatial Fourier transform of the Lorentz force generated by different meander coils is used to determine the optimal driving frequency for single mode generation. The numerical calculation is used to characterize the new magnetic configuration and the conventional EMAT magnet. Experimental examinations of each meander coil in combination with the conventional and new magnetic configuration show that the Lamb wave signal can be selectively enhanced by choosing the appropriate driving frequency and coil parameters through using the improved meander-coil EMAT.

Keywords: Lamb wave, selective enhancement, meander-coil, electromagnetic acoustic transducer (EMAT)

PACS: 43.20.–f, 43.35.–c **DOI:** 10.1088/1674-1056/27/8/084301

1. Introduction

Ultrasonic testing methods are effectively used in industrial nondestructive testing. An electromagnetic acoustic transducer (EMAT) is a kind of non-contact ultrasonic transducer that does not require a liquid couplant, and can be convenient and flexible to generate various types of ultrasonic waves to meet different ultrasonic testing requirements. They can be used in special environments such as high temperature, high speed, and the isolation layer.[1,2] As is well known, the Lamb wave technique has been widely used in nondestructive testing and evaluating (NDT & E) of the plate-like structure. According to the wave structure and the different forms of particle vibrations, Lamb waves can be classified as symmetric modes (S0, S1, S2, ...) and antisymmetric modes (A0, A1, A2, ...). Because a Lamb wave contains multiple modes, it is difficult to analyze and we cannot take full advantage of its multi-mode properties.[3,4] This will hinder the application of the Lamb wave EMAT detection technique, which usually requires the selective generation of a single pure Lamb wave mode. Therefore, it is of great significance for finding a method to control or regulate the generation of Lamb wave modes. Moreover, the main disadvantage of using EMATs is their poor transduction efficiency compared with the piezoelectric transducers, so their signal-to-noise ratio (SNR) is relatively low. This drawback severely restricts the application of EMATs in various fields.[5] Therefore, there is a need to design the EMATs with a higher signal-to-noise ratio and pure ultrasonic wave. In order to try to improve the signal-to-noise performance of EMAT, a lot of work has been done. The researchers established the mathematical model of EMATs and made significant progress of theoretical analyses and numerical simulation.[6–12] At present, there is little research on Lamb wave mode selection. Li *et al.* provided a theoretical and experimental basis to selectively generate a single and pure Lamb wave mode by using EMATs, which showed the influences of the coil parameters and driving frequency on mode selection.[3,4]

In this paper, we focus on how to selectively enhance the Lamb mode signal amplitude. A single and pure Lamb wave mode can be selectively generated at a certain driving frequency when the coil parameters are given. Wave structure analysis shows that the magnetic field direction has an influence on the generation of different Lamb wave modes. We use a new magnetic configuration in which both horizontal and perpendicular magnetic fields are enhanced to increase the transduction efficiencies for different Lamb modes. Such a magnetic configuration has been combined with the racetrack coil into an EMAT for body waves,[13] and it was also combined with a meander line coil to enhance surface wave conduction efficiency,[14] but has not been used for Lamb wave signals. Finally, some experimental examinations are carried out to verify the performance of the improved meander-coil EMAT.

2. Theoretical fundamentals

2.1. Wave structure analysis

The wave structure refers to the distribution of the physical quantities such as displacement, stress, and strain along

*Project supported by the National Natural Science Foundation of China (Grant Nos. 51507171 and 51577184).
†Corresponding author. E-mail: liuguoqiang@mail.iee.ac.cn
© 2018 Chinese Physical Society and IOP Publishing Ltd

the thickness of the plate. The wave structure characteristics of the Lamb wave show the vibration of the particles along the thickness direction and the Lamb wave energy distribution.[15] Combined with the characteristic equation of Lamb wave and wave structure theory, the normalized displacement wave structure of aluminum Lamb wave can be obtained.[15] Figure 1 shows the normalized displacement wave structures of Lamb wave A0 and S0 mode at 400 kHz in a 3-mm-thick aluminum plate with a longitudinal speed of 6350 m/s and a transverse speed of 3100 m/s. It can be seen from Fig. 1(a) that in the plate thickness range, u_x is symmetrical with respect to the origin, and u_z is symmetrical with respect to the straight line where the displacement of plate thickness is taken as 0. The u_x and u_z represent the in-plane displacement and the out-of-plane displacement, respectively, indicating the displacement of the Lamb wave in the propagation direction of the aluminum plate and the displacement of the Lamb wave in the thickness direction of the aluminum plate. The magnitude of u_z is greater than u_x. The u_x reaches a maximum on the upper and lower surfaces of the plate, and it is zero at the center of the plate. It can be seen from Fig. 1(b) that in the plate thickness range, u_z is symmetrical with respect to the origin, and u_x is symmetrical with respect to the straight line where the displacement of plate thickness is taken as 0. The magnitude of u_x is greater than u_z. The u_z reaches the maximum on the upper and lower surfaces of the plate, and it is zero at the center of the plate.

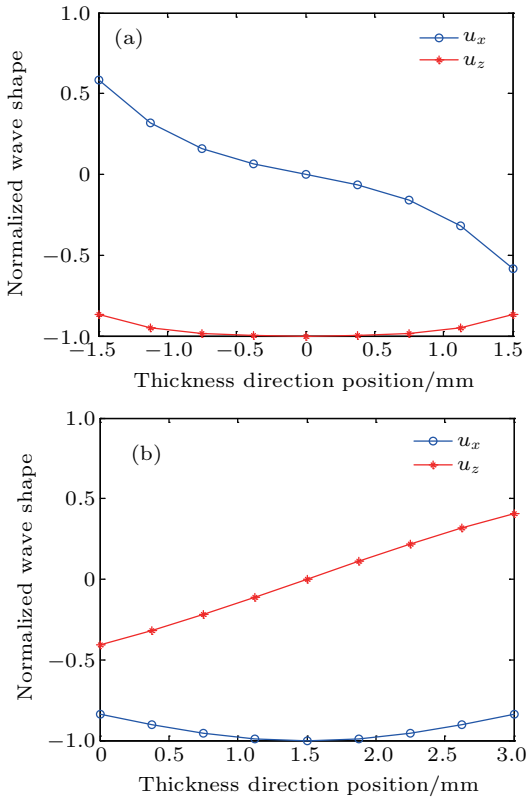


Fig. 1. (color online) Normalized displacement wave structures of Lamb wave at 400 kHz in 3 mm-thick aluminum plate: (a) A0 mode, and (b) S0 mode.

The amplitude of in-plane displacement of the S0 mode is large, and the out-of-plane displacement is almost zero. The A0 mode is dominated by out-of-plane displacement, and both the in-plane displacement and out-of-plane displacement amplitude of the A0 mode are large. Therefore, the perpendicular magnetic field can more easily generate the S0 mode, and the horizontal magnetic field can more easily generate the A0 mode. This is of great significance for selecting the mode and improving the efficiency of electromagnetic acoustic transduction.

2.2. Mode selective generation and numerical analysis

When the EMAT technique is operated on a non-ferromagnetic material, only the Lorentz force mechanism needs to be considered. The two-dimensional model of the meander-coil EMAT that generates Lamb waves in an aluminum plate is shown in Fig. 2, where the thickness of the aluminum plate is $2d$, the oz axis indicates the Lamb wave propagation direction, and the oy axis indicates the direction of the plate thickness. The permanent magnet is placed above the meander coil and the static bias magnetic field B_s is applied to the meander coil. Figure 2(a) shows that a perpendicular static bias magnetic field generated by the permanent magnet is applied to the meander coil, and the Lorentz force generated by the perpendicular static magnetic field is along the horizontal direction. Figure 2(b) shows the horizontal static bias magnetic field generated by the permanent magnets is applied to the meander coil, and the Lorentz force generated by the horizontal static magnetic field is along the perpendicular direction. The parameter a represents the width of the meander coil single wire, D denotes the spatial period of the meander coil, and L refers to the total length of the meander coil. The parameter g represents the lift-off distance and is assumed to remain constant throughout the analyses.

An alternating current $i(t) = I\exp(\mathrm{j}\omega t)$ is applied to the meander coil, where the angular frequency $\omega = 2\pi f$, f is the driving frequency. It is assumed that the Lorentz force P_{zy} becomes zero outside the EMAT coverage ($z \in (-L/2, L/2)$). The spatial Fourier transform of P_{zy} is given by (omitting the factor $\exp(\mathrm{j}\omega t)$):[3,4,16]

$$\begin{aligned} P^*_{zy}(k) &= \frac{1}{2\pi}\int_{-L/2}^{L/2} P_{zy}\exp(-\mathrm{j}kz)\,\mathrm{d}z \\ &= \frac{B_s Ik}{2\pi a}\sum_n \frac{A_n}{k^2-\xi_n^2}\left[\exp(q_n\delta)-1\right] \\ &\quad\times\exp\left[-\xi_n(h+d)\right]\left[\cos\left(\frac{\xi_n L}{2}\right)\sin\left(\frac{kL}{2}\right)\right. \\ &\quad\left.-\frac{\xi_n}{k}\sin\left(\frac{\xi_n L}{2}\right)\cos\left(\frac{kL}{2}\right)\right], \end{aligned} \tag{1}$$

where $A_n = 4\sin[(2n+1)\pi a/D]/(2n+1)\pi$, $\xi_n = 2\pi(2n+1)/D$, $\delta = \sqrt{2/\omega\eta\bar{\mu}_{zz}}$, and $q_n = \sqrt{(\bar{\mu}_{zz}/\bar{\mu}_{yy})\xi_n^2 + 2\mathrm{j}/\delta^2}$, $n =$

$(0,1,2,\ldots)$, with $\mathrm{Re}(q_n) < 0$, parameter $\bar{\mu}_{rr}(r = y,z)$ representing the relative magnetic permittivity, η being the conductivity of the plate material, and k the wave-number equal to $2\pi/D$.[3,4]

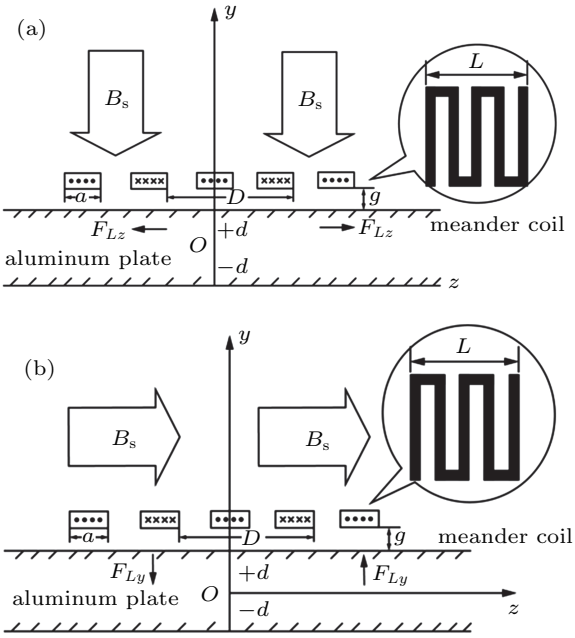


Fig. 2. Two-dimensional model of EMAT for generating Lamb waves: (a) perpendicular static bias magnetic field, and (b) horizontal static bias magnetic field.

In the numerical analyses, the thickness of the aluminum plate is 3 mm. When the driving frequency f is 510 kHz, the phase velocity c_p of A0 mode is 2554 m/s and the phase velocity c_p of S0 mode is 5130 m/s. According to the phase velocity and the driving frequency, we can obtain the spacing between adjacent wires generating a single A0 mode to be $c_\mathrm{p}/2f = 2554/(2\times 510\ \mathrm{kHz}) = 2.5$ mm and the spacing between adjacent wires generating single S0 mode to be 5 mm. The corresponding D values are 5 mm and 10 mm. Because the ultrasonic wave amplitude reaches its maximum value when the magnet length is three times the meander-coil length,[14] we choose the meander-coil length to be 15.2 mm (the length of magnet is 40 mm). We separately calculated and analyzed two meander-coils with $a = 0.2$ mm, $L = 15.2$ mm, and $g = 0.5$ mm, but $D = 5$ mm and 10 mm. When $D = 5$ mm, we call its corresponding coil No. 1, and when $D = 10$ mm, we call its corresponding coil No. 2.

When the geometrical parameters of the meander coils are given, the curve of the spatial Fourier transform, denoted by $P^*_{zy}(k)$, of the Lorentz force $P_{zy} = P_{zy}(z)$ exerted on the aluminum plate $(y = +d)$ is calculated by Eq. (1) and shown on the left side of Figs. 3(a) and 3(b), and n is selected to be 7.[4] The dispersion curves (wave-number k versus f) of Lamb wave in a 3-mm thick aluminum plate are simultaneously shown on the right side of each of Figs. 3(a) and 3(b). Both the $P^*_{zy}(k)$ curve and the Lamb wave dispersion curve have the same wave-number axis. The displacement field of the n-th Lamb wave mode is proportional to the magnitude of the spatial transform of $P_{zy}(z)$ under $k = k_n$. According to Fig. 3, the magnitudes of the n-th Lamb wave modes corresponding to different given frequencies can be obtained.

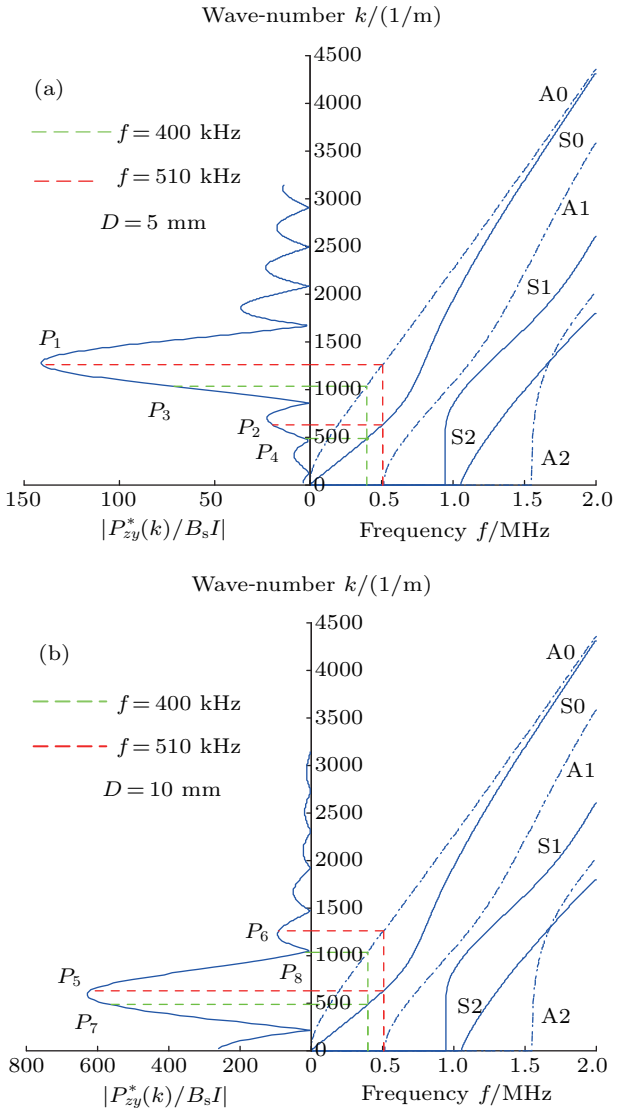


Fig. 3. (color online) Curves of the spatial Fourier transform of the Lorentz force (left) and Lamb wave dispersion curves (right) in each panel: (a) EMAT with coil No. 1, and (b) EMAT with coil No. 2.

It can be seen from Fig. 3(a) that when the driving frequency of the meander coil No. 1 is $f = 510$ kHz (given by the red dashed line), the Lamb wave A0 and S0 modes may be generated. The corresponding magnitudes of $P^*_{zy}(k_n)$ that contribute to the generation of the A0 and S0 modes, are determined by points P_1 and P_2 in Fig. 3(a). The meander coil No. 1 is designed based on the phase velocity of the A0 mode at the driving frequency $f = 510$ kHz, and the amplitude of the A0 mode is close to the main lobe peak at this moment. However, the amplitude of S0 mode is also large at the same time. When the driving frequency is adjusted to $f = 400$ kHz (given by the green dashed line in Fig. 3(a)), the A0 and S0 mode may be generated. The corresponding mag-

nitudes of $P^*_{zy}(k_n)$ that contribute to the generation of the A0 and S0 modes are determined by points P_3 and P_4 in Fig. 3(a). Clearly, the magnitude of $P^*_{zy}(k_n)$ for the generation of the A0 mode (determined by point P_3) is far larger than that of the S0 mode (determined by point P_4). Therefore, the A0 mode will play a dominant role and the S0 mode will be restrained at the frequency $f = 400$ kHz. When the driving frequency of the meander-coil No. 2 is $f = 510$ kHz (given by the red dashed line in Fig. 3(b)), the Lamb wave S0 and A0 mode will be also simultaneously generated. The corresponding magnitudes of $P^*_{zy}(k_n)$ that contribute to the generation of the A0 and S0 modes, are determined by points P_5 and P_6 in Fig. 3(b). The meander coil No. 2 is designed based on the phase velocity of the S0 mode at the driving frequency $f = 510$ kHz and the amplitude of S0 mode is close to the main lobe peak at this time. However, the amplitude of the A0 mode is also large at the same time. This does not exert a very good suppression effect on the A0 mode. It can be seen from Fig. 3(b) that when the driving frequency is adjusted to $f = 400$ kHz, the magnitude of $P^*_{zy}(k_n)$ for the generation of the S0 mode (determined by point P_7) is much larger than that of the A0 mode (determined by point P_8), and it can be considered that there will be only the S0 mode, and the A0 mode will be suppressed at this time.

2.3. Static magnetic field modeling

In this subsection, the magnetic flux density profiles of the conventional and the new magnetic configuration will be obtained by simulation. The three-dimensional (3D) finite element model (FEM) is established with Maxwell. The conventional magnetic configuration is generally used as EMATs in combination with meander-coils as shown in Fig. 4(a). The improved EMAT is designed as shown in Fig. 4(b), and the magnetic configuration consists of two identical square magnets side by side with opposite polarity. Both EMATs use the meander-coils with the same length L and width b, and the same magnetic material, NdFeb (grade: N35).

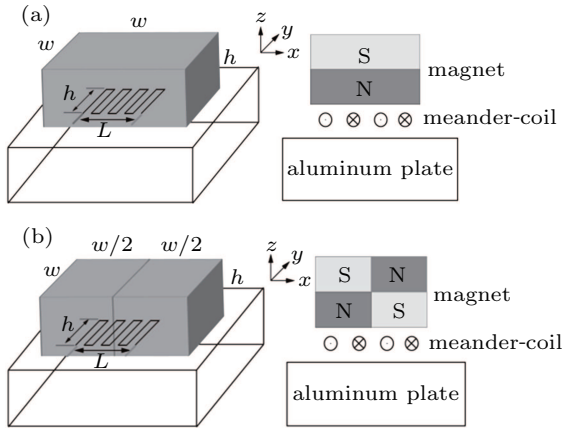


Fig. 4. Comparison of the magnetic configuration of EMATs between (a) conventional EMAT, and (b) improved EMAT with the new magnetic configuration.

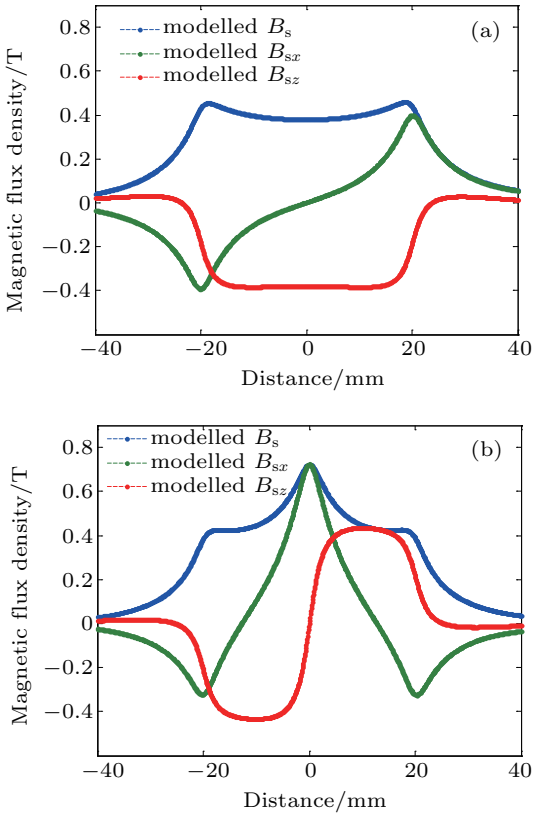


Fig. 5. (color online) Modelled magnetic flux density curves for (a) conventional and (b) new EMAT magnetic configuration.

The space volume ($w \times w \times h$) of the magnet in the conventional EMAT is the same as the space volume of the magnet in the improved EMAT. The dimension of the magnet in the conventional EMAT is 40 mm×40 mm×20 mm, and the dimension of each magnet in the improved EMAT is 40 mm×20 mm×20 mm. The residual magnetic flux intensity in magnets is set to be 1.18 T for both cases. Figures 5(a) and 5(b) show the magnetic flux density profile on a 2-mm line just below the center of the conventional and new magnetic configurations. It can be seen from Fig. 5(a) that the horizontal component of the magnetic flux density B_{sx} is equal to zero at the center and reaches two peaks near the two edges of the magnet. The perpendicular component of the magnetic flux density B_{sz} has a flat peak under the magnet surface. Therefore, the total magnetic flux density B_s is slightly larger near the edges of the magnet. It can be seen from Fig. 5(b) that the horizontal component of the magnetic flux density B_{sx} has a maximum at the center of the magnets, and two local peaks at the two edges of the magnets. The perpendicular component of the magnetic flux density B_{sz} is zero at the center and has two flat peaks under each magnet surface. Therefore, the total magnetic flux density B_s has a large peak at the center and two local peaks at the two edges of the magnets. According to the magnet simulation results, the conventional EMAT magnetic field direction is mainly perpendicular to the meander

coil. The magnetic flux density of the magnet in the improved EMAT has both horizontal and perpendicular magnetic flux on the meander coil, and the horizontal magnetic field is stronger. It can also be observed that in the central area where the meander coil is located, the magnetic flux density of the improved EMAT magnet has a much larger peak in Fig. 5(b) than the maximum in Fig. 5(a).

3. Experimental validation

Some experiments are carried out to validate the performance of the improved EMAT and the above theoretical analyses. The experimental setup for Lamb waves is illustrated in Fig. 6. The dimension of the conventional EMAT magnet and the improved EMAT magnet are exactly the same as those used in the above simulation. The meander coils of the two EMATs (transmitter and receiver) are fabricated by the printed circuit board (PCB) technique. The parameters of the meander coils used in the EMATs are also the same as those used in the above numerical analysis, and their geometrical parameters are $a = 0.2$ mm, $D = 5$ mm and $D = 10$ mm, $L = 15.2$ mm, and $g = 0.2$ mm. The EMATs are applied by a burst current signal with 7 cycles at the driving frequency $f = 0.4$ MHz to generate and receive Lamb waves in an aluminum plate (1000 mm×1000 mm×3 mm) with the RITEC RAM-5000-SNAP system. The whole system operates in a transmitter-receiver mode. The separation distance of the EMAT transmitter and receiver is set to be 300 mm.

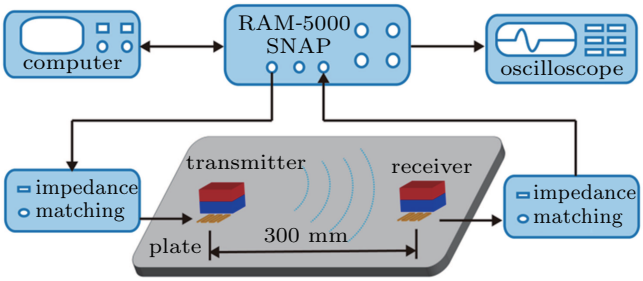


Fig. 6. (color online) Experimental setup for Lamb wave generation and measurement with EMATs.

3.1. Lamb waves generated by EMAT at frequency $f = 400$ kHz under conventional magnetic configuration

According to the wave structure analysis results (shown in Fig. 1), the A0 and S0 modes may be generated by the EMAT transmitter at the driving frequency $f = 400$ kHz. When the conventional magnet and the coil No. 1 are combined into an EMAT, the magnitude of the generated A0 mode signal will be larger than that of the S0 mode, which is shown in Fig. 3(a). When the conventional magnet and coil No. 2 are combined into an EMAT, the magnitude of the generated S0 mode signal will be larger than that of the A0 mode in Fig. 3(b). Figures 7(a) and 7(b) show the time-domain ultrasonic pulse signals detected by the conventional magnetic configuration with coil No. 1 and coil No. 2 when the spatial separation between the centers of the two transducers (transmitter and receiver) is set to be 300 mm.

There is one ultrasonic pulse signal in Fig. 7(a) or Fig. 7(b), and the corresponding arriving times are around 110 μs and 80 μs. When the driving frequency $f = 400$ kHz, the theoretical group velocities of the A0 and S0 modes are 3142 m/s and 4923 m/s, respectively. Thus, the theoretical arriving times of the A0 and S0 mode signal should be 96 μs and 61 μs. Because the burst wave signal has a time delay about 12 μs, the signal in Fig. 7(a) should be the A0 mode signal and the signal in Fig. 7(b) should be the S0 mode signal.

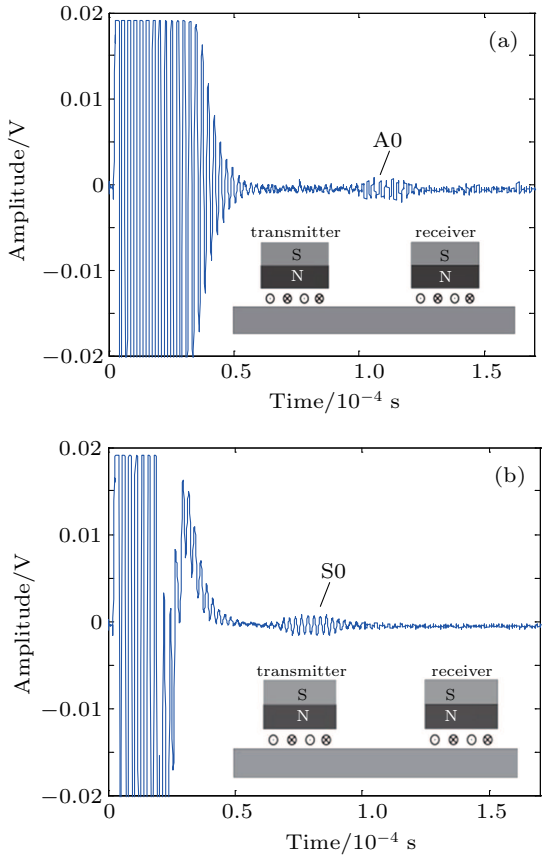


Fig. 7. (color online) Conventional EMATs with (a) coil No. 1, and (b) coil No. 2 as transmitter and receiver at driving frequency $f = 400$ kHz.

3.2. Lamb waves generated by EMAT at frequency $f = 400$ kHz under new magnetic configuration

Figure 8 shows the time-domain ultrasonic pulse signals detected by the new magnetic configuration with coil No. 1 and No. 2. There are two ultrasonic pulse signals in Fig. 8(a) and one ultrasonic pulse signal in Fig. 8(b). The corresponding arriving times are around 80 μs and 110 μs in Fig. 8(a) and the corresponding arriving time is around 80 μs. When the driving frequency $f = 400$ kHz, the theoretical arriving times of

the A0 and S0 mode signal should be 96 μs and 61 μs. Because the burst wave signal has a time delay of about 12 μs, the signal in Fig. 8(a) should contain the S0 mode and A0 mode, and the signal in Fig. 8(b) should be the S0 mode signal.

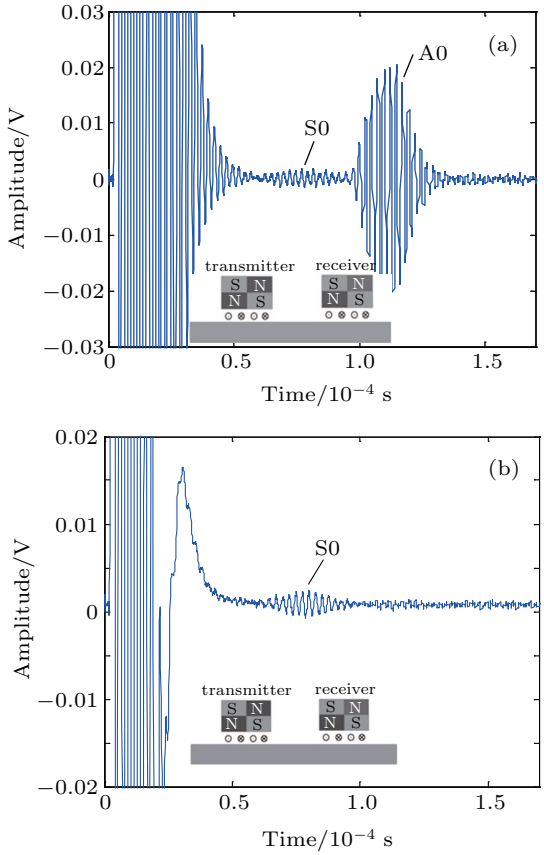


Fig. 8. (color online) Improved EMATs with (a) coil No. 1, and (b) coil No. 2 as transmitter and receiver at driving frequency $f = 400$ kHz.

The Lamb wave S-series mode (S0, S1, S2, ...) is dominated by in-plane displacement, and the A-series mode (A0, A1, A2, ...) is dominated by out-of-plane displacement. Therefore, the perpendicular magnetic field can more easily generate the S-series mode, and the horizontal magnetic field can more easily generate the A-series mode. Since coil No. 1 is designed based on the phase velocity of the A0 mode, the horizontal magnetic field plays a dominant role regardless of the magnetic configuration. Similarly, since coil No. 2 is designed based on the phase velocity of the S0 mode, the perpendicular magnetic field plays a major role. Through the analysis of the above experimental results, we can see that the experimental conditions in Figs. 7(b) and 8(b) are the same, except that the magnetic configuration is different. Both magnetic configurations have the same space volume, and the meander coil is placed in the center of the magnetic configuration and the coil length is 1/3 of the magnet length. When combined with a conventional magnet, the meander coil is mainly subjected to a perpendicular magnetic field and the horizontal magnetic field is small. When combined with the new magnetic configuration, the meander coil is primarily affected by a relatively large horizontal magnetic field and is also affected by the perpendicular magnetic field. However, for coil No. 2, the perpendicular magnetic field plays a major role. The perpendicular magnetic field generated by the new magnetic configuration is larger than that generated by the conventional magnet in the area where the coils are placed. Therefore, the signal amplitude in Fig. 8(b) is slightly larger than that in Fig. 7(b). The signals in Figs. 7(a) and 8(a) are obtained by combining No. 1 coil and different magnetic configurations into EMATs. In Fig. 7(a), the A0 mode signal is weak, and the A0 mode signal of Fig. 8(a) is much larger than the S0 mode signal. Since the coil No. 1 is designed based on the phase velocity of the A0 mode, the horizontal field plays a major role in generating the A0 mode. When No. 1 coil is combined with the conventional magnet, the horizontal magnetic field in the area where the coil is located is small, so the A0 mode signal in Fig. 7(a) is very small. When coil No. 1 is combined with the new magnetic configuration, the area where the coil is located is subjected to a strong horizontal magnetic field and also a strong perpendicular magnetic field. Therefore, the signal in Fig. 8(a) has two modes, and the S0 mode is very small. In the previous numerical analysis of Fig. 3(a), it can be seen that when the driving frequency of coil No. 1 is 400 kHz, the S0 mode is suppressed and the amplitude is still small despite being affected by the strong perpendicular magnetic field. Therefore, for these two cases, experimental results and theoretical analyses are in good agreement.

4. Conclusions

In order to make full use of each mode of Lamb wave, a method to selectively enhance the single mode signal of the Lamb wave is proposed. Lamb waves have multiple modes, and in this paper we use the simplest A0 and S0 modes as examples for investigation. First, the parameters of the coils generating a single mode are determined based on the wave structures and the phase velocities of different modes. Then the optimal driving frequency is determined based on the analytical expression of the Lorentz force's spatial Fourier transform amplitude. The simulation is used to calculate the magnetic flux distributions of the new magnetic configuration and the conventional one. The horizontal magnetic field and perpendicular magnetic field of the new magnetic configuration are all larger than those of the conventional magnet. Finally, each coil with conventional and new magnetic configuration is combined into an EMAT experimentally. The experimental results show that the Lamb wave signal can be selectively enhanced by selecting an appropriate driving frequency and coil parameters through using the improved meander-coil EMAT.

References

[1] Petcher P A, Potter M D G and Dixon S 2014 *NDT & E International* **65** 1

[2] Kogia M, Gan T H, Balachandran W, Livadas M, Kappatos V, Szabo I, Mohimi A and Round A 2016 *Sensors* **16** 582

[3] Li M L, Deng M X and Gao G J 2014 *Chin. J. Acoust.* **33** 156

[4] Li M L, Deng M X and Gao G J 2016 *Chin. Phys. B* **25** 124301

[5] Mirkhani K, Chaggares C, Masterson C, Jastrzebski M, Dusatko T, Sinclair A, Shapoorabadi R, Konrad A and Papini M 2004 *NDT & E International* **37** 181

[6] Wang S J, Su R L, Chen X Y, Kang L and Zhai G F 2013 *IEEE Trans. Ultra. Ferro. Freq. Control* **60** 2657

[7] Thring C B, Fan Y and Edwards R S 2016 *NDT & E International* **81** 20

[8] Jian X, Dixon S, Grattan K T V and Edwards R S 2006 *Sensors Actuators A* **128** 296

[9] Kang L, Wang S J, Jiang T and Zhai G F 2011 *Jpn. J. Appl. Phys.* **50** 7S

[10] Wang S J, Kang L, Li Z C, Zhai G F and Zhang L 2012 *Mechatronics* **22** 653

[11] Kang L, Dixon S, Wang K C and Dai J M 2013 *NDT & E International* **59** 11

[12] Kang L, Zhang C, Dixon S, Zhao H, Hill S and Liu M H 2017 *NDT & E International* **86** 36

[13] Ohtaki K, Uchimoto T and Takagi T 2010 *Int. J. Appl. Electromag. Mech.* **33** 1135

[14] Pei C X, Zhao S Q, Xiao P and Chen Z M 2016 *Sensors Actuators A: Phys.* **247** 539

[15] Wang S, Huang S L and Zhao W 2009 *J. Tsinghua Univ. (Sci. & Tech.)* **49** 909

[16] Masahiko H and Hirotsugu O 2003 *EMATs for Science and Industry on contacting Ultrasonic Measurements* (Boston: Kluwer Academic Publishers)